Chin. Geogra. Sci. 2013 Vol. 23 No. 4 pp. 460–469
doi: 10.1007/s11769-013-0601-1

Springer Science Press
www.springerlink.com/content/1002-0063

A Thin Cloud Removal Method from Remote Sensing Image for Water Body Identification

ZHENG Wei[1], SHAO Jiali[1], WANG Meng[1], HUANG Dapeng[2]

(1. *National Satellite Meteorological Center*, *Beijing* 100081, *China*; 2. *National Climate Center*, *Beijing* 100081, *China*)

Abstract: In this paper, a thin cloud removal method was put forward based on the linear relationships between the thin cloud reflectance in the channels from 0.4 μm to 1.0 μm and 1.38 μm. Channels of 0.66 μm, 0.86 μm and 1.38 μm were chosen to extract the water body information under the thin cloud. Two study cases were selected to validate the thin cloud removal method. One case was applied with the Earth Observation System Moderate Resolution Imaging Spectroradiometer (EOS/MODIS) data, and the other with the Medium Resolution Spectral Imager (MERSI) and Visible and Infrared Radiometer (VIRR) data from Fengyun-3A (FY-3A). The test results showed that thin cloud removal method did not change the reflectivity of the ground surface under the clear sky. To the area contaminated by the thin cloud, the reflectance decreased to be closer to the reference reflectance under the clear sky after the thin cloud removal. The spatial distribution of the water body area could not be extracted before the thin cloud removal, while water information could be easily identified by using proper near infrared channel threshold after removing the thin cloud. The thin cloud removal method could improve the image quality and water body extraction precision effectively.

Keywords: thin cloud removal; water body; Moderate Resolution Imaging Spectroradiometer (MODIS); Medium Resolution Spectral Imager (MERSI); Visible and Infrared Radiometer (VIRR)

Citation: Zheng Wei, Shao Jiali, Wang Meng, Huang Dapeng, 2013. A thin cloud removal method from remote sensing image for water body identification. *Chinese Geographical Science*, 23(4): 460–469. doi: 10.1007/s11769-013-0601-1

1 Introduction

Water body is a significant parameter for earth surface environment, climate change and flood disaster monitoring. Satellite remote sensing technology can play an important role in water body monitoring and assessment because of its ability of quickly acquiring wide range of earth surface information, including areas being hard to reach (Zheng, 2008). Optical remote sensing data, such as Moderate Resolution Imaging Spectroradiometer (MODIS) and Advanced Very High Resolution Radiometer (AVHRR), have had many successful application cases for water body monitoring (Barton and Bathols, 1989; Sheng *et al.*, 1998; Sheng *et al.*, 2001; Bryant and Rainey, 2002; Zhan *et al.*, 2002; Peng *et al*., 2004; Cai *et al.*, 2005; Jain *et al.*, 2006; Huang *et al.*, 2008). But for the optical remote sensing data, only cloud-free images are required to monitor the water under a clear sky. However, there is little clear sky during the flood, and cloud contamination will result in invalidation of optical remote sensing data. If the water body information under the cloud can be extracted, it will be a great significant thing. For optical remote sensing data, when affected by the thick clouds, the ground information can not be got only using the image itself; when affected by thin cloud, part of the energy reflected by surface can get through the thin cloud and reach the sensor. In this case, the surface object, especially the water body, can be identified after removing the impact of thin cloud.

Many removal methods for thin cloud have been

Received date: 2012-03-12; accepted date: 2012-08-10
Foundation item: Under the auspices of National Nature Science Foundation of China (No. 40901231, 41101517)
Corresponding author: Zheng Wei. E-mail: azheng1125@163.com

studied so far. Tasseled-cap transformation was an orthogonal transformation of the original data into new multi-dimensional space. To the Landsat/MSS or TM images contaminated by the cloud, the fourth tasseled-cap band was mainly taken as the noise (cloud). Then, the first three tasseled-cap bands were transformed back to RGB image which had removed the impact of cloud (Richter, 1996; Ma and Gu, 2005). But this method would lead to the loss of band information and be unfit to the image with some bright subjects. The algorithm based on wavelet theory was used to remove the cloud (Tseng *et al.*, 2008; Zhu *et al*., 2009). The algorithm could make earth surface information and cloud noises distributed to the coefficients of low levels and high levels respectively. Most of cloud noises and some useful information were included in high level coefficients where cloud was brighter than the surface information. Cloud could be removed from these coefficients and information. Weight factors were assigned to the detailed coefficients of low level, high level, and approximation coefficients respectively for enhancing the contrast of earth surface and decreasing remaining cloud. The three parts of coefficients were reconstructed and fused to get processed results. The homomorphism filtering method had also been used to remove the thin cloud because the thin cloud was the low frequency component in remote sensing images (Zhao and Zhu, 1996). However, the above methods all changed the physical information of the original image, which made the quantitative analysis difficult. An improved homomorphism filtering method was adopted to remove thin cloud qualitatively at first, and all bands were selected to classify pixels (Feng *et al*., 2004; Ma and Gu, 2005). Based on the fact that visible band images contained more aerosol effects than infrared bands, visible bands were used to determine clear or hazy regions and the reflectance of different surface classes in clear regions were calculated. At last the mean reflectance of the same classes in clear and hazy regions was matched to remove cloud. Atmospheric correction methods could remove the effects of aerosol, cloud and water vapor (Liang *et al.*, 2001; Liang *et al.*, 2002; Juan *et al.*, 2010), and met the requirements of quantitative analysis to some extent, while its computation was too complicated to execute.

Based on the above analysis, we can know that there is not a proper thin cloud removal method for easily and quickly extracting water information from the remote sensing image contaminated by the thin cloud. In this paper, we put forward an effective and easy thin cloud removal method according to the spectral characteristics of water body, atmosphere and thin cloud, and the relationships between the thin cloud reflectance of the channels from 0.4 μm to 1.0 μm and 1.38 μm. The thin cloud removal method can be used to improve the image quality and water body extraction precision for flood disaster monitoring and water resource management.

2 Materials and Methods

2.1 Study area

In this paper, for researching the effectiveness of the thin removal method, two study areas were chosen. The first study area is within the Huaihe River Basin (Fig. 1), with 800 km in length and 400 km in width, covering 270 000 km^2. Huaihe River is the sixth largest river in China, located in the middle eastern part of China. In recent 20 years, three severe floods have happened respectively in 1991, 2003 and 2007. The disaster has made many adverse impacts on economic development in this region. For the first study area, Earth Observation System Moderate Resolution Imaging Spectroradiometer (EOS/MODIS) data was applied.

The second study area was situated within the Danjiangkou Reservoir (Fig. 1). Danjiangkou Reservoir is a multi-purpose reservoir, located in Xichuan County of Henan Province and Danjiangkou City of Hubei Province, central China. It was constructed in 1958, created by the Danjiangkou Dam, and at the time was one of the largest reservoirs in Asia. The Danjiangkou Reservoir is the water source for one of the routes of the ′South to North Water Transfer Project′, providing water to Beijing and Tianjin. Moreover, it serves as a water supply for the local region, as well as irrigation, electricity generation and flood control. For this study area, Fengyun-3A (FY-3A) Medium Resolution Spectral Imager (MERSI) and Visible and Infrared Radiometer (VIRR) data were used.

It is quite significant to monitor the two study areas by using satellite remote sensing data for flood disaster prevention and water resource management.

2.2 Data and processing

2.2.1 MODIS data and processing

The MODIS instrument has a viewing swath width of

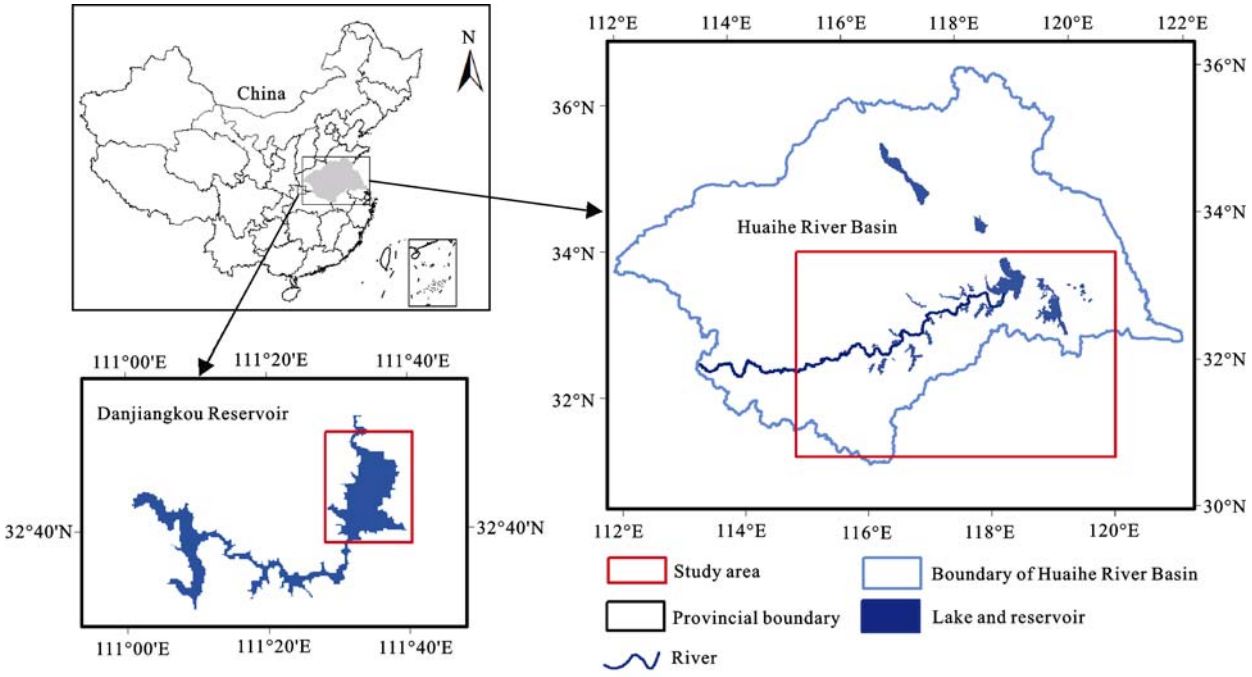

Fig. 1 Sketch map of study areas

2330 km and scans the entire surface of the Earth every one to two days. Its detectors measure 36 spectral bands between 0.405 μm and 14.385 μm, including two channels of 0.66 μm and 0.86 μm with 250 m resolution, five channels with 500 m resolution and 29 channels with 1 km resolution (Justice *et al*., 1998; Liu and Ge, 2000; Liu and Yang, 2004). MODIS data with the spatial resolution from hundred meters up to kilometer, and the temporal resolution of two or more days, have the irreplaceable ability of quickly assessing and mapping surface water body. In this paper, 0.66 μm, 0.86 μm and 1.38 μm channels will be applied to identifying the water body under the thin cloud. In order to match the 250 m spatial resolution of the 0.66 μm and 0.86 μm channels, 1.38 μm channel with 1 km resolution was resampled to 250 m. The MODIS images contaminated by the thin cloud on June 25, 2003 in the Huaihe River Basin were selected as the test data.

2.2.2 FY-3A data and processing

The development of China′s new generation of polar-orbiting meteorological satellite series FY-3A greatly enhances the surface monitoring ability, meanwhile provides a new data source for water body monitoring for large area. Medium Resolution Spectral Imager (MERSI) as one of the 11 instruments on board the FY-3A satellite has five channels with 250 m spatial resolution (including 0.66 μm and 0.86 μm channels) and 15 channels with 1 km resolution. MERSI has both multi-spectral and high spatial resolution properties, which greatly improves the ability to observe fine surface features (Dong *et al*., 2009; Yang *et al*., 2009). Therefore, MERSI instrument has greater potential to provide the ideal data sources for flood and water resource monitoring. Visible and Infrared Radiometer (VIRR) on board the FY-3A satellite has the 1.38 μm channel with 1 km resolution. VIRR and MERSI have the same scene time and area, so VIRR can detect the cloud information when MERIS data is used to map water body. For matching the spatial resolution of the MERSI data, 1.38 μm channel of VIRR was resampled to 250 m resolution. The FY-3A images contaminated by the thin cloud for the Danjiangkou Reservoir on May 4, 2011 were chosen as the second test data.

2.3 Methods

2.3.1 Cloud detection

Cloud detection is the first step to remove the influence of cloud. Confirmation of thin cloud region can avoid the correction of the free-cloud area. Thin cloud consists of ice particles having different sizes and shapes. The ′effective′ particle sizes (radii of equivalent spheres) are usually greater than 5 μm. The ice particles in the spectral range of 0.4–1.0 μm are much larger than wavelengths and ice is non-absorbing. Weak ice absorptions

occur near 1.24 μm and 1.38 μm. The 1.38 μm channel has strong capabilities of thin cloud detection (Ackerman *et al*., 1998; Liu and Yang, 2004). The reflectances at 1.38 μm are smaller than reflectances in the 0.4–1.0 μm spectral mainly because of absorption by water vapor above and within the cirrus clouds (Gao *et al*., 1998). Water vapor almost abstracts all the spectral energy, most of reflectance come from the high-altitude thin cirrus in the 1.38 μm channel. The thin cloud information can be extracted easily through setting threshold value in the 1.38 μm channel (Ackerman *et al*., 1998), so the threshold method was employed to distinguish the thin cloud in this paper (Equation (1)).

$$T_{\mathrm{L\_1.38}} > R_{1.38} > T_{\mathrm{M\_1.38}} \tag{1}$$

where $T_{\mathrm{L\_1.38}}$ is the threshold value between cloud and clear sky in the 1.38 μm channel; $R_{1.38}$ is the reflectance in the 1.38 μm channel; $T_{\mathrm{M\_1.38}}$ is the threshold value between thin cloud and thick cloud in the 1.38 μm channel.

However, 1.38 μm is not sensitive to all types of cloud, while 0.66 μm can be utilized to detect the thick cloud which have higher reflectance than other surface objects in the visible channel (Chen *et al*., 2002), so the threshold of 0.66 μm will be added to distinguish the thick cloud from other objects, the expression is as follows.

$$R_{0.66} < T_{0.66} \tag{2}$$

where $R_{0.66}$ is the reflectance in the 0.66 μm channel; $T_{0.66}$ is the threshold value between thick cloud and clear sky in the 0.66 μm channel.

2.3.2 Thin cloud removal

Hypothesizing that atmosphere in the study area is homogeneous, we think that the effect of atmosphere is much smaller than thin cloud for water extraction. So, surface reflection and atmospheric scattering to the sensor are considered together, expressed as $L_{\mathrm{s+a}}$ (Zheng *et al.*, 2007). Thus, radiation brightness (L^*) received by the sensor can be considered primarily including two components (Fig. 2), cloud reflection (L_{c}), and surface reflection and atmospheric scattering ($L_{\mathrm{s+a}}$), then L^* can be expressed as:

$$L^* = L_{\mathrm{c}} + L_{\mathrm{s+a}} \tag{3}$$

For a flat and Lambertian surface, L^* can be expressed as:

$$L^* = \frac{\cos\theta \times E \times R^*}{\pi} \tag{4}$$

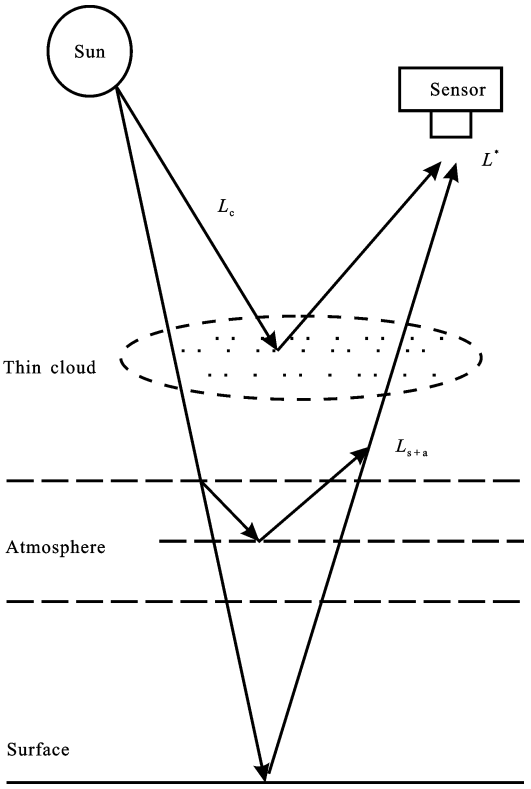

Fig. 2 Diagram of satellite observation principle under thin cloud sky

where R^* is the apparent reflectance; E is the exoatmospheric solar irradiance; θ is the sun zenith angle.

L_{c} can be calculated by the following equation:

$$L_{\mathrm{c}} = \frac{\cos\theta \times E \times R_{\mathrm{c}}}{\pi} \tag{5}$$

where R_{c} is the reflectance of thin cloud.

$L_{\mathrm{s+a}}$ can be expressed as:

$$L_{\mathrm{s+a}} = T_{\mathrm{c}} \times \frac{\cos\theta \times E \times R_{\mathrm{s+a}}}{\pi} \tag{6}$$

where T_{c} is the thin cloud transmittance; $R_{\mathrm{s+a}}$ is the reflectance of surface and atmosphere.

From equations (3) to (6), we can obtain the following expression.

$$R^* = R_{\mathrm{c}} + T_{\mathrm{c}} \times R_{\mathrm{s+a}} \tag{7}$$

The previous researchers found that there was a good linear relationships between the thin cloud reflectance of the channels from 0.4 μm to 1.0 μm and the 1.375 μm channel of AVIRIS data (Gao *et al.*, 1998; Gao and Li, 2000). The reflectance of thin cloud can be expressed

as:

$$R_{c(\lambda)} = \frac{R_{c(1.38)}}{k} \quad (8)$$

where $R_{c(\lambda)}$ is the reflectance of thin cloud in band length λ; $R_{c(1.38)}$ is the reflectance of thin cloud in the 1.38 μm; k is the empirical coefficient which can be got by the reflectance relationships of 1.38 μm, visible and near infrared channels (Gao *et al.*, 1998);

T_c reflects the transmittance of thin cloud, which can be calculated by:

$$T_c = (1 - \frac{R_{c(1.38)}}{k})^n \quad (9)$$

where n is an experiential parameter with a typical value between 1 and 2, which depends on both the solar and sensor geometries.

To remote sensing data, it is more difficult to distinguish water body from other surface objects in the visible channel than in the near infrared channel. Using the threshold value method, water body information can be extracted easily in the near infrared channel. Because 0.86 μm is sensitive to the water body, and has a good relationship with the 1.38 μm channel, therefore, 0.86 μm was chosen as the main channel to extract water body information in this paper.

3 Results and Analyses

3.1 Thin cloud removal from MODIS image

Figure 3 showed that the west part of MODIS image on June 25, 2003, was contaminated severely by cloud. Firstly, we used 1.38 μm channel to detect cloud. However, 1.38 μm channel was not sensitive to all kinds of clouds. Thick cloud at the middle-east part of image in 0.66 μm could be seen obviously (Fig. 3a), but almost invisible in 1.38 μm (Fig. 3b). So the cloud undetected by 1.38 μm was identified by 0.66 μm (channel 1) effectively based on the Equation (2).

For accurately detecting the cloud covered area, the selection of threshold value is important. Referring to the spectra curve of thick and thin clouds (Gao *et al.*, 1998; Gao and Li, 2000), for 1.38 μm channel, 0.01 was selected as the threshold value to distinguish cloud and cloud-free areas, and 0.13 was selected as the threshold value to distinguish thin cloud and thick cloud. For 0.66 μm channel, 0.30 was selected as the threshold value to detect the thick cloud.

Figure 4 showed the scatter map of images in the 0.86 μm and 1.38 μm channels. The X axis mainly represented the surface reflectance, and Y axis indicated the cloud reflectance. The left scatter points reflected the relationship between lower surface reflectance and thin cloud was chosen to estimate k value, which was set as 0.7. It is noted that if selected k value is higher, then the corrected surface reflectance will be lower, and if selected k value was smaller, the correction of thin cloud was not enough. By comparing the same surface type reflectance under clear sky and thin cloud, T_c could be estimated, and then n was estimated to be equal to 1 according to several experiments based on the Equation (9).

Figure 5 showed the images comparison results before and after the thin cloud removal. It was very obvious that the image after the thin cloud removal became clearer, which indicated that the thin cloud removal

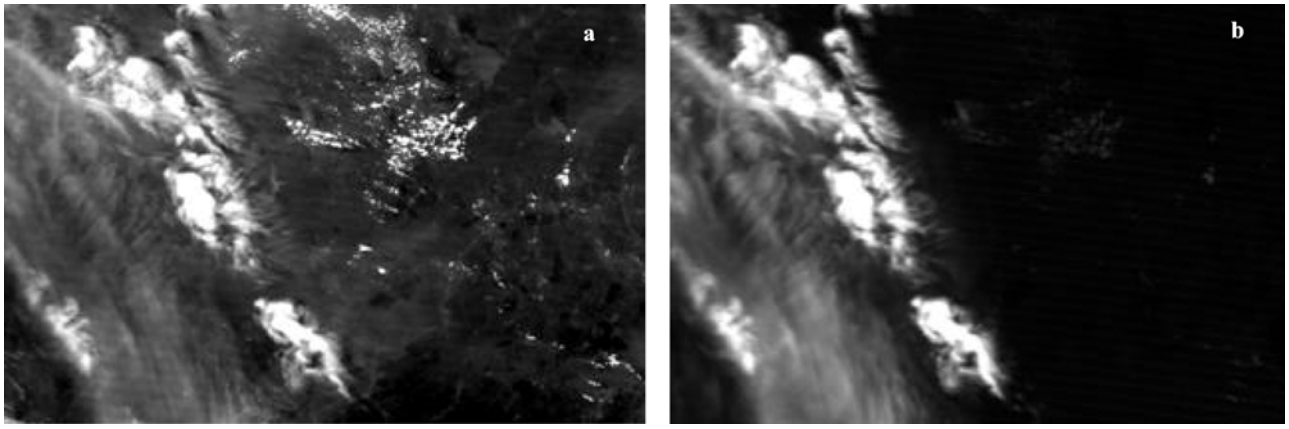

Fig. 3 MODIS images in 0.66 μm (a) and 1.38 μm (b) channels in Huaihe River Basin

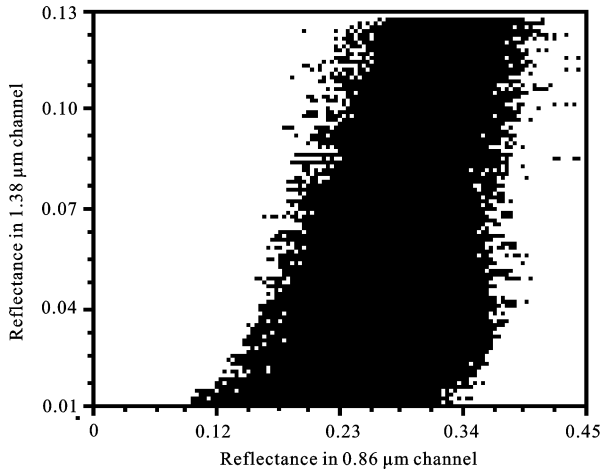

Fig. 4 Reflectance scatter map in 1.38 μm and 0.86 μm channels in Huaihe River Basin

method could improve the image quality clearly. In the *X*-axis direction of the image, a profile line (the first 480 lines) was selected for profile analysis and the results were shown in the Fig. 6. Through profile analysis, we knew that the algorithm did not change the surface reflectance under clear sky. To the area contaminated by the thin cloud, the reflectance decreased after the thin cloud removal, which proved the efficiency of thin cloud removal method.

In order to verify the impact of classification before and after the thin cloud removal, a sub-area image in the Huaihe River Basin contaminated by the thin cloud in the 0.86 μm was chosen as the test area shown in Fig. 7. Threshold method was employed to classify the two images before and after the thin cloud removal (Fig. 7a, 7b). In the classification process, we found that the threshold method was invalid and could not extract the exact spatial distribution of the water body area before the thin cloud removal; while water information could easily be identified after the thin cloud removal by using threshold method (Fig. 7c). An image under the clear sky on June 28, 2003 was selected to extract water body

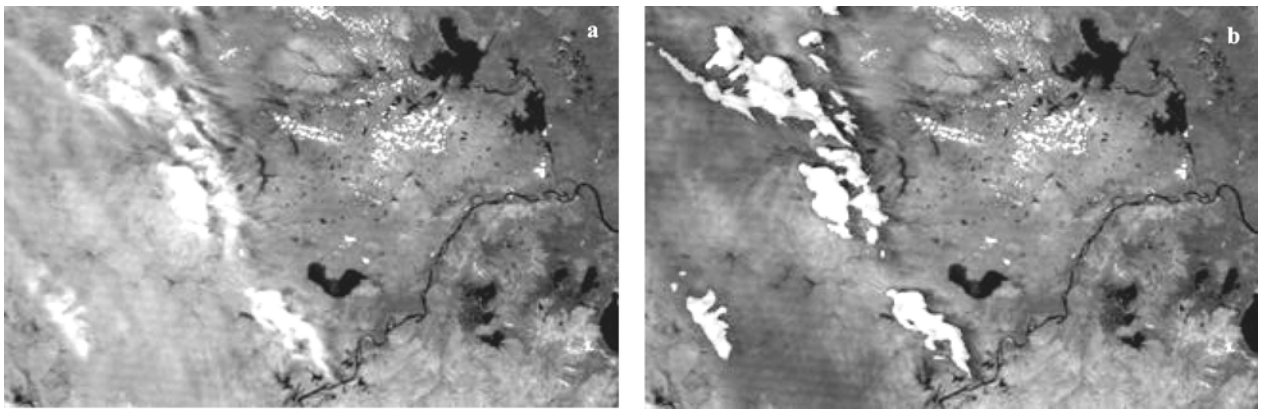

Fig. 5 Comparison of MODIS images in 0.86 μm before (a) and after (b) thin cloud removal in Huaihe River Basin

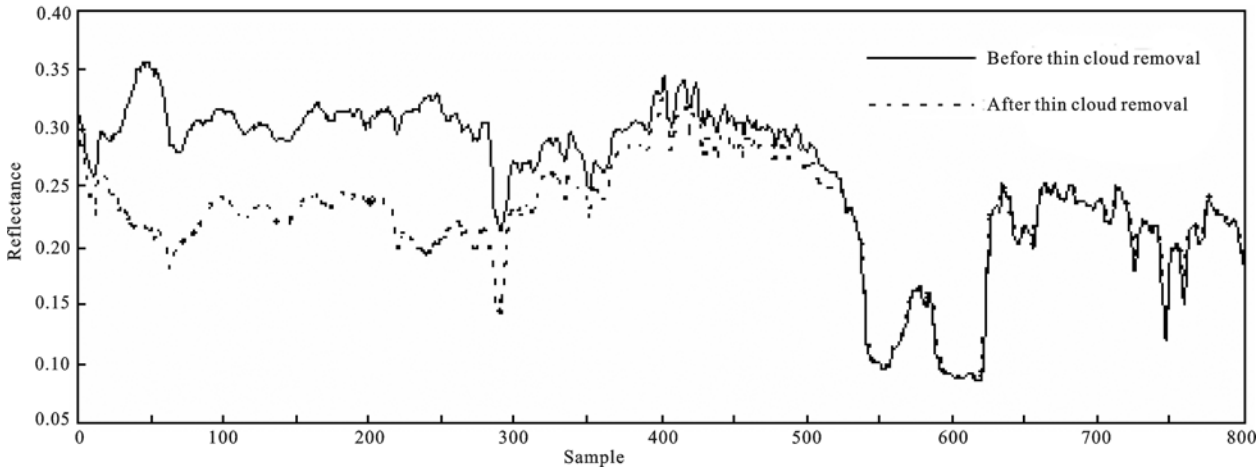

Fig. 6 Reflectance comparison of image in 0.86 μm before and after thin cloud removal in Huaihe River Basin

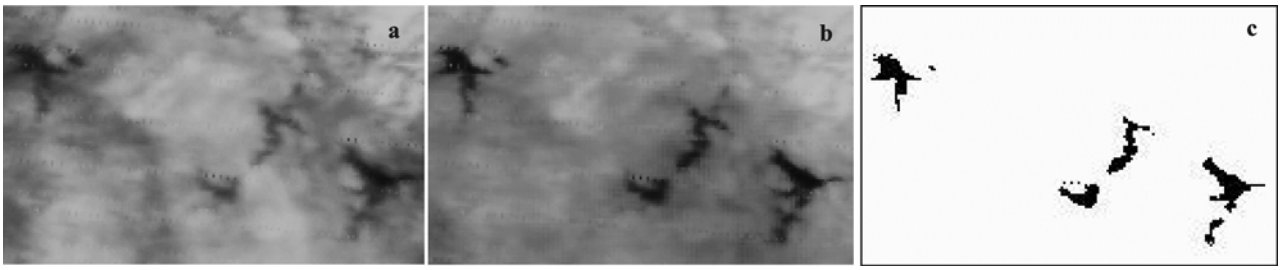

Fig. 7 Comparison of images in 0.86 μm before (a) and after (b) thin cloud removal and classification images after removal (c) in Huaihe River Basin

area as the reference value. By comparison, water body classification accuracy after the thin cloud removal reached to 91.3%.

Comparison of surface reflectance before and after the thin cloud removal can reflect the effect of thin cloud removal. The clear sky image on June 28, 2003 was selected as the reference reflectance to compare with the water reflectance before and after the thin cloud removal, as shown in Table 1. The reflectance before the thin cloud removal was significantly higher than the reference value under the clear sky. After the thin cloud removal, the reflectance value of water was closer to the reference reflectance.

Table 1 Comparison of water reflectance before and after the thin cloud removal and under clear sky

Reflectance	Time of image capture	Value
Before thin cloud removal	June 25, 2003	0.204
After thin cloud removal	June 25, 2003	0.134
Reference value	June 28, 2003	0.078

3.2 Thin cloud removal from MERSI and VIRR images

Based on the thin cloud removal method, we used MERSI and VIRR images to extract the water body information in the Danjiangkou Reservoir on May 4, 2011. Detailed process of the thin cloud removal was similar to that for MODIS images. The parameter k was estimated to be 0.4, and n was equal to 1. Compared with the image under the clear sky on May 4, 2011, the image after the thin cloud removal became clearer in the south-west region of the reservoir (Fig. 8), which indicated that image quality was improved. Figure 8 obviously showed that quality of image was better after the thin cloud removal, and water information could be easily extracted by threshold method, which indicated the thin cloud removal method was reliable for FY-3 data.

For quantitatively describing the effect of thin cloud removal to FY-3 image, three representative samples were chosen (Table 2). The image under clear sky image on May 5, 2011 was selected as the reference reflectivity,

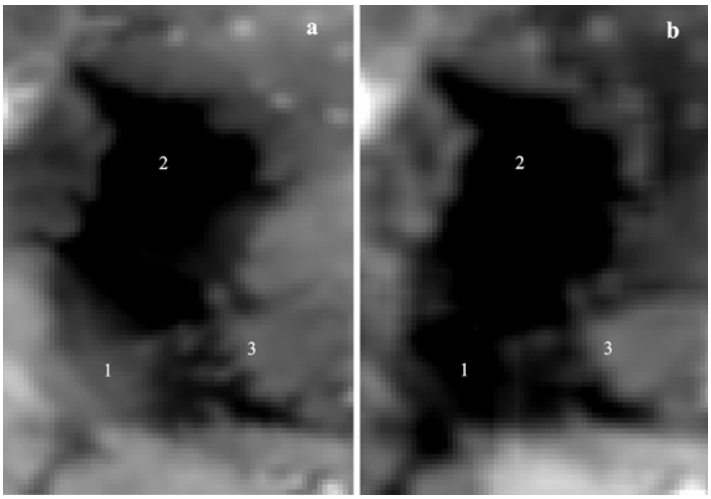

Fig. 8 Comparison of 0.86 μm images of FY-3A/MERSI before (a) and after (b) thin cloud removal on May 4, 2011 in Danjiangkou Reservoir (1, 2 and 3 represent samples′ location)

to compare with the surface reflectance before and after the thin cloud removal, as shown in Table 2. The reflectance before the thin cloud removal was significantly higher than reference reflectivity under the clear sky. After the thin cloud removal, values of the first and third sampling points values were closer to the reference reflectance. The second sampling point did not changed because no thin cloud contamination. This point value was much higher than reference reflectance under the clear sky because of atmospheric scattering. The comparison result indicated effectiveness of the thin cloud removal method.

Table 2 Comparison of surface reflectance before and after thin cloud removal and under clear sky

Sampling point	Reflectance before thin cloud removal	Reflectance after thin cloud removal	Reference reflectance under clear sky
1	0.26	0.16	0.06
2	0.17	0.17	0.06
3	0.29	0.25	0.24

Note: locations of sampling points 1, 2 and 3 were showed in Fig. 8

4 Discussion

Both MODIS and MERSI data, with the spatial resolution from hundred meters up to kilometers, and the temporal resolution of two or more days, have the irreplaceable ability of quickly assessing and mapping the flood and water. Under the thick cloud, the ground information can not be got by using the optical remote sensing data, while multi-sensor data involving optical and microwave data can resolve this problem effectively. When the optical remote sensing data are affected by the thin cloud, part of the energy reflected by surface can get through it and reach the sensor, and then ground information can be got by using the thin cloud removal method.

Atmospheric correction could remove the effects of aerosol, cloud and water vapor. But the computation procedures was quite complicated. In order to easily and quickly extract water information, although we possibly get better result after atmospheric correction, the effect of atmosphere is much smaller than thin cloud for water extraction. So, supposed that atmosphere in the study area is homogeneous, surface reflection and atmospheric scattering to the sensor are both considered. This ensured that we focused on the thin cloud removal and did not attempt to correct the atmospheric effect.

Cloud detection is the first step for removing the effect of cloud. Water vapor almost abstracts all the spectral energy, most of reflectance come from the high-altitude thin cirrus in the 1.38 μm channel. The 1.38 μm has been used to detect the high-altitude thin cirrus. The 0.66 μm channel was utilized to distinguish the thick cloud with higher reflectance than other surface objects. To determine the threshold value, the spectra curve of thick and thin clouds were referred. Application of more channels such as near 3.7 μm and 12.0 μm may improve the cloud detection precision. The study about cirrus ice particle size, shape, and orientation distributions, spatial variability, and scattering phase functions were not sufficient for reliable modeling of cirrus reflectivity. Cirrus effects were difficult to simulate by using radiative transfer model. So, the empirical relationships were selected to characterize the main cirrus properties. In the thin cloud removal method, k and n were empirical coefficients, different data have different k and n values, which possibly brought the errors into the thin cloud removal model, so the calibration of the two coefficients needs numerous experiments. It will be our main efforts to quantify the parameters in the further work.

5 Conclusions

The simple thin cloud removal method was proposed based on the linear relationships between the thin cloud reflectance of the channels from 0.4 μm to 1.0 μm and 1.38 μm. In order to validate the effectiveness of this method for different areas and data, two application examples were given, one was for EOS/MODIS data and the other was for FY-3A/MERSI and VIRR data. According to the results of extracting the water body information, it can be concluded that the impact of cloud has been weakened after the thin cloud removal, whist the data of the area without the thin cloud did not be changed. The thin cloud removal algorithm could meet the requirements of quantitative analysis for further analyses. The image quality after the thin cloud removal was obviously better than that before the thin cloud removal. Before the thin cloud removal, the threshold method was invalid and could not extract the exact spatial distribution of the water body area when image classification; while water information could easily be identified by using threshold method after the thin cloud

removal. The application results indicated that thin cloud removal model was effective to improve the quality of EOS/MODIS, FY-3A/MERSI and VIRR images as well as the water body extraction precision, which promoted the application of China′s polar-orbiting meteorological satellite FY-3.

References

Ackerman S A, Strabala K I, Menzel W P *et al.*, 1998. Discriminating clear sky from clouds with MODIS. *Journal of Geophysical Research*, 103(D24): 32141–32157. doi: 10.1029/1998JD200032

Barton I J, Bathols J M, 1989. Monitoring foods with AVHRR. *Remote Sensing of Environment*, 30: 89–94. doi: 10.1016/0034-4257(89)90050-3

Bryant R G, Rainey M P, 2002. Investigation of flood inundation on playas within the Zone of Chotts, using a time-series of AVHRR. *Remote Sensing of Environment*, 82(2–3): 360–375. doi: 10.1016/S0034-4257(02)00053-6

Cai Y L, Sun G Q, Liu B Q, 2005. Mapping of water body in Poyang Lake from partial spectral unmixing of MODIS data. *International Geoscience and Remote Sensing Symposium*, 7: 4539–4540. doi: 10.1109/IGARSS.2005.1526675

Chen P Y, Srinivasan R, Fedosejevs G *et al.*, 2002. An automated cloud detection method for daily NOAA-14 data for Texas, USA. *International Journal of Remote Sensing*, 23(15): 2939–2950. doi: 10.1080/01431160110075631

Dong C H, Yang J, Yang Z D *et al.*, 2009. An overview of a new chinese weather satellite FY-3A. *Bulletin of the American Meteorological Society*, 90: 1531–1544.

Feng C, Ma J W, Dai Q *et al*., 2004. An improved method for cloud removal in ASTER data change detection. *IEEE International Geoscience and Remote Sensing Symposium*, 5: 3387–3389. doi: 10.1109/IGARSS.2004.1370431

Gao B C, Kaufman Y J, Han W *et al*., 1998. Correction of thin cirrus path radiance in the 0.4–1.0 μm spectral region using the sensitive 1.375 μm cirrus detecting channel. *Journal of Geophysical Research*, 103: 32169–32176

Gao B C, Li R R, 2000. Quantitative improvement in the estimates of NDVI values from remotely sensed data by correcting thin cirrus scattering effects. *Remote Sensing of Environment*, 74(3): 494–502.

Huang Dapeng, Liu Chuang, Fang Huajun *et al.*, 2008. Assessment of waterlogging risk in Lixiahe Region of Jiangsu Province based on AVHRR and MODIS image. *Chinese Geographical Science*, 18(2): 178–183. doi: 10.1007/s11769-008-0178-2

Jain S J, Saraf A J, Ajanta G *et al*., 2006. Flood inundation mapping using NOAA/AVHRR data. *Water Resource Manage*, 20(6): 949–959. doi: 10.1007/s11269-006-9016-4

Juan C, Jiménez-Muñoz, José A *et al.*, 2010. Atmospheric correction of optical imagery from MODIS and reanalysis atmospheric products. *Remote Sensing of Environment*, 114(10): 2195–2210. doi: 10.1016/j.rse.2010.04.022

Justice C O, Vermote E, Townshend J R G *et al.*, 1998. The Moderate Resolution Imaging Spectroradiometer (MODIS): Land remote sensing for global change research. *IEEE Transctions on Geoscience and Remote Sensing*, 36(4): 1228–1249. doi: 10.1109/36.701075

Liang S L, Fang H L, Chen M Z, 2001. Atmospheric correction of Landsat ETM+ land surface imagery. I. Methods. *IEEE Transctions on Geoscience and Remote Sensing*, 39(11): 2490–2498. doi: 10.1109/36.964986

Liang S, H Fang, Morisette J T *et al*., 2002. Atmospheric correction of Landsat ETM+ land surface imagery. II. Validation and Applications. *IEEE Transctions on Geoscience and Remote Sensing*, 40(12): 2736–2746. doi: 10.1109/TGRS.2002.807579

Liu Chuang, Ge Chenghui, 2000. Characteristics and application of remote sensed data from U.S. EOS-MODIS. *Remote Sening Information*, 3: 45–48. (in Chinese)

Liu Yujie, Yang Zhongdong, 2004. *MODIS Remote Sensing Information Processing Principle and Algorithm*. Beijing: Science Press. (in Chinese)

Ma Jianwen, Gu Xingfa, 2005. Chun Study of thin cloud removal method for CBERS-02 image. *Science in China* (*Series E*), 35: 89–86. (in Chinese)

Peng Dingzhi, Guo Shenglian, Huang Yufang, 2004. Flood disaster monitoring and assessing system based on MODIS and GIS. *Journal of Wuhan University of Hydraulic and Electric Engineering*, 37: 7–11. (in Chinese)

Richter R, 1996. A spatially adaptive fast atmospheric correction algorithm. *International Journal of Remote Sensing*, 17(6): 1201–1214. doi: 10.1080/01431169608949077

Sheng Y W, Su Y F, Xiao Q G, 1998. Challenging the cloud-contamination problem in flood monitoring with NOAA/AVHRR imagery. *Photogrammetric Engineering and Remote Sensing*, 64(3): 191–198.

Sheng Y, Gong P, Xiao Q, 2001. Quantitative dynamic flood monitoring with NOAA AVHRR. *International Journal of Remote Sensing*, 22(9): 1709–1724. doi: 10.1080/01431160118481

Tseng D C, Tseng H T, Chien C L, 2008. Automatic cloud removal from multi-temporal SPOT images. *Applied Mathematics and Computation*, 205(2): 584–600.

Yang Jun, Dong Chaohua, Lu Naimeng *et al*., 2009. FY-3A: The new generation polar-orbiting meteorological satellite of China. *Acta Meteorologica Sinica*, 67(4): 501–509. (in Chinese)

Zhan X, Sohlberg R A, Townshend J R G *et al.*, 2002. Detection of land cover changes using MODIS 250 m data. *Remote Sensing of Environment*, 83(1–2): 336–350. doi: 10.1016/S0034-4257(02)00081-0

Zhao Zhongming, Zhu Chongguang, 1996. Approach to removing cloud cover from satellite imagery. *Remote Sensing of Environment China*, 11(3): 195–199. (in Chinese)

Zheng Wei, 2008. *Multi-Source Remote Sensing Data Mining for Flood Monitoring Systematically—A Case Study in Huaihe River Basin*. Beijing: Institute of Geographic Sciences and Natural Resources Research, Chinese Academy of Sciences. (in Chinese)

Zheng W, Liu C, Zeng Z Y *et al*., 2007. A feasible atmospheric correction method to TM image. *Journal of China University of Mining and Technology*, 17(1): 112–115.

Zhu Xifeng, Wu Fang, Tao Chunkan, 2009. A new algorithm of cloud removing for optical images based on wavelet threshold theory. *Acta Photonica Sinica*, 38(12): 3312–3317. (in Chinese)